ACS OMEGA

http://pubs.acs.org/journal/acsodf

Article

Electronic, Thermal, and Thermoelectric Transport Properties of ε-Ga_2O_3 from First Principles

Qingsong Liu, Zimin Chen, and Xianzhong Zhou*

Cite This: *ACS Omega* 2022, 7, 11643−11653

Read Online

ACCESS | Metrics & More | Article Recommendations | Supporting Information

ABSTRACT: The electronic, thermal, and thermoelectric transport properties of ε-Ga_2O_3 have been obtained from first-principles calculation. The band structure and electron effective mass tensor of ε-Ga_2O_3 were investigated by density functional theory. The Born effective charge and dielectric tensor were calculated by density perturbation functional theory. The thermal properties, including the heat capacity, thermal expansion coefficient, bulk modulus, and mode Grüneisen parameters, were obtained using the finite displacement method together with the quasi-harmonic approximation. The results for the relationship between the Seebeck coefficient and the temperature and carrier concentration of ε-Ga_2O_3 are presented according to the ab initio band energies and maximally localized Wannier function. When the carrier concentration of ε-Ga_2O_3 increases, the electrical conductivity increases but the Seebeck coefficient decreases. However, the figure of merit of thermoelectric application can still increase with the carrier concentration.

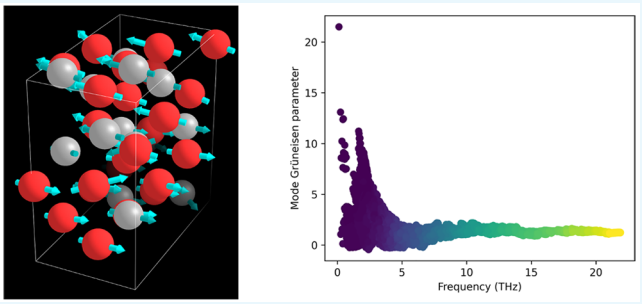

1. INTRODUCTION

Ga_2O_3 is an emerging wide-band-gap material for semiconductor power devices due to its high breakdown voltage.[1] Ga_2O_3 also exhibits transparency for the UV region, which makes it a promising material for application in optoelectronics, such as a solar blind deep-UV photodetector.[2,3] Although Ga_2O_3 has broad application prospects, the fundamental properties are still poorly understood due to its polymorphism.[4] Ga_2O_3 can form several polymorphs, denoted as α-Ga_2O_3, β-Ga_2O_3, γ-Ga_2O_3, δ-Ga_2O_3, and ε-Ga_2O_3,[5,6] which makes the characteristics of Ga_2O_3 very complex. Recently, ε-Ga_2O_3 thin films were successfully grown on various substrates.[7−10] It has been proved that an epitaxial ε-Ga_2O_3 thin film can be thermally stable up to nearly 1000 K.[11] Table 1 shows the phase transition temperatures in a dry atmosphere of these five Ga_2O_3 phases, which was measured by Roy et al.[5] Theoretical calculations by Yoshioka et al. indicated that the formation energy of these phases is in the order $\beta < \varepsilon < \alpha < \delta < \gamma$.[12] Although β-Ga_2O_3 is the most stable at room temperature, ε-Ga_2O_3 can be stable up to 1000 K, which makes it a promising material for application in electronic devices. To date, a lot of the properties of Ga_2O_3 come from theory, such as density functional theory (DFT), because it is not easy to prepare high-quality pure Ga_2O_3 samples for measurement.[13]

An essential factor to consider in high-power electronic applications is the heat dissipation of the devices. Compared with other wide-band-gap semiconductors, such as GaN and GaAs, the thermal conductivity of Ga_2O_3 is much smaller and thus a clear weak point of Ga_2O_3 in terms of power device application.[14] The details of electrical transport and energy dissipation could help us develop high-performance electronic devices. Hence, it becomes crucial to understand the details of the thermal and thermoelectric properties of ε-Ga_2O_3. The latest studies on the transport and thermoelectric properties of β-Ga_2O_3 show numerical values for the Seebeck coefficient and power factor, which encourages more research on further improvements of Ga_2O_3. To the best of our knowledge, to date, no specific theoretical research on the thermoelectric properties of ε-Ga_2O_3 based on ab initio electronic structure calculations combined with Boltzmann transport equations has appeared, and only some experiments related to the electron

Table 1. Transformation Relationship among Five Different Phases of Ga_2O_3[5]

phase transition	temperature
δ-$Ga_2O_3 \rightarrow \varepsilon$-$Ga_2O_3$	773 K
α-$Ga_2O_3 \rightarrow \beta$-$Ga_2O_3$	873 K
γ-$Ga_2O_3 \rightarrow \beta$-$Ga_2O_3$	923 K
ε-$Ga_2O_3 \rightarrow \beta$-$Ga_2O_3$	1143 K

Received: November 12, 2021
Accepted: March 21, 2022
Published: March 31, 2022

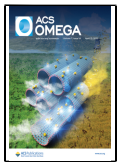

transport and thermoelectric properties are available. In this paper, we attempt and summarize the results of the theoretical derivation of the transport and thermoelectric properties of ε-Ga_2O_3 using the semiclassical Boltzmann transport theory.

2. RESULTS AND DISCUSSION

2.1. Electronic Properties. The optimized unit cell of ε-Ga_2O_3 with 40 atoms is shown in Figure 1, which is rendered

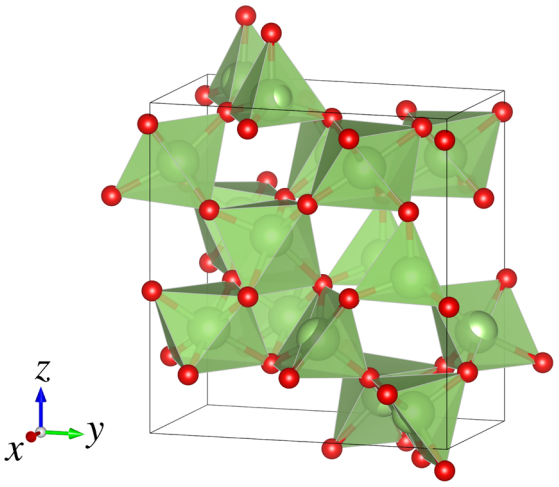

Figure 1. Optimized atomic structure of ε-Ga_2O_3, where the large atoms are gallium and the small red atoms are oxygen.

by VESTA.[15] The optimized lattice parameters of ε-Ga_2O_3 are a = 5.12 Å, b = 8.79 Å, and c = 9.41 Å, which are 1.5%, 1.0%, and 1.4% larger than the experimental values by Cora et al.[10] but consistent with previous theoretical values by Yoshioka et al.[12]

The calculated electron band structure along with the Brillouin zone, the total density of states (DOS), and the projection density of states (PDOS) are presented in Figure 2. The band structure is interpolated by the Wannier function. From the band structure and DOS shown in Figure 2, it can be seen that the energy positions of each group of bands (representing O 2s, Ga 3d, and O 2p in the higher part of the valence band and Ga 4s, Ga 4p, and Ga 4d in the lower part of the conduction band) are rather similar to the band structures of β-Ga_2O_3. This is clearly reflected in the DOS. The band gap of ε-Ga_2O_3 is about 4.9 eV as determined by optical spectra, which is comparable to that of β-Ga_2O_3.[7,16] Our calculated direct band gap at the zone center is 2.11 eV, underestimating the expected experimental band gap of DFT.[17] However, the calculated band gap of ε-Ga_2O_3 is closest to the value of β-Ga_2O_3 (see Supporting Information Note II). The effective electron mass tensor is defined by[18]

$$\left(\frac{1}{m^*}\right)_{ij} = \frac{1}{\hbar^2}\frac{\mathrm{d}^2 E_C}{\mathrm{d}k_i \mathrm{d}k_j} \tag{1}$$

where E_C is the dispersion of the lowest conduction band and k_i and k_j are the ith and jth elements of $\mathbf{k}$, respectively. If the conduction band minimum is E_0 and it locates at point Γ then the first-order approximation of E_C can be expressed as

$$E_C \approx E_0 + \frac{1}{2}\hbar^2 \sum_{i=1}^{3}\sum_{j=1}^{3} m_{i,j}^{*-1} k_i k_j \tag{2}$$

In order to obtain the effective electron mass tensor, the band structure of ε-Ga_2O_3 was first calculated by Quantum ESPRESSO with a coarse $\mathbf{k}$ mesh. Then, the band structure of ε-Ga_2O_3 was interpolated by Wannier90 using a maximally localized Wannier function. Considering that a good quadratic fit requires very dense sampling at different directions in k space close the center of the Brillouin region, the spacing is the reciprocal of the lattice constant of 0.002. Finally, eq 2 was used to fit the interpolated band structure near the conduction band minimum using the Scikit-Learn python package, yielding the inverse mass tensor. Then, we can invert this tensor to obtain the mass tensor itself as follows

$$m^* = \begin{pmatrix} 0.219 & 0.000 & 0.000 \\ 0.000 & 0.216 & 0.000 \\ -0.002 & -0.001 & 0.215 \end{pmatrix} m_0 \tag{3}$$

where m_0 is the free electron mass. The electron effective mass of ε-Ga_2O_3 is quite isotropic with an average value of $0.217m_0$,

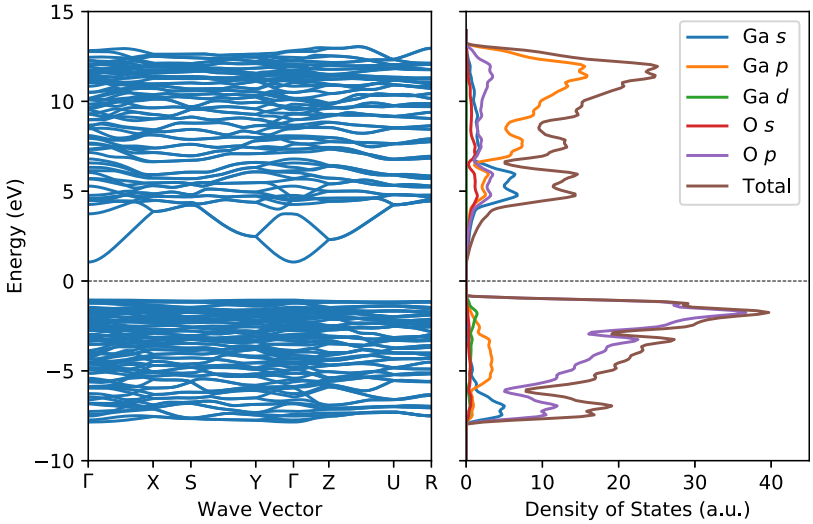

Figure 2. Dispersion relation (left) and densities of states (right) of electrons in ε-Ga_2O_3. Gray dashed lines indicate the Fermi levels, which are set at the center of the band gap.

https://doi.org/10.1021/acsomega.1c06367
ACS Omega 2022, 7, 11643−11653

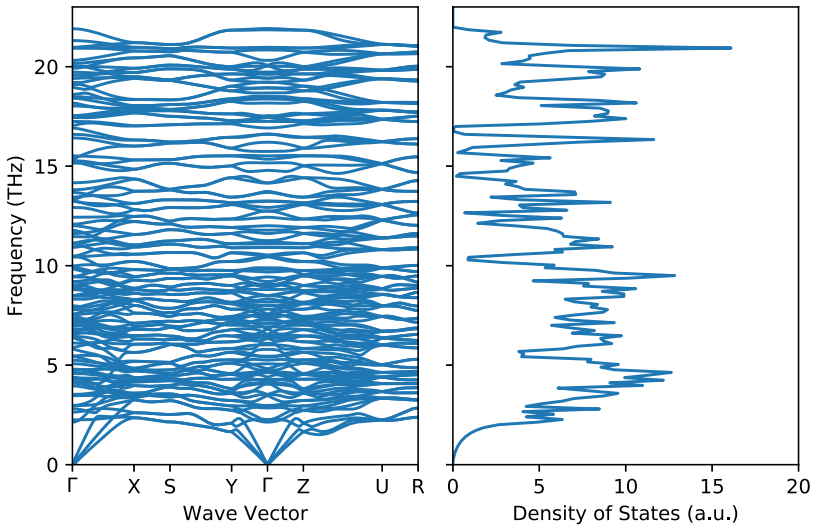

Figure 3. Dispersion relation (left) and densities of states (right) of phonon in ε-Ga_2O_3.

which is quite close to the effective mass of β-Ga_2O_3 (see Supporting Information eq S1). Due to the strong Ga−O ionic bond, the energy distribution of the empty and occupied electronic states is little affected by the actual arrangement of the Ga and O atoms.

2.2. Thermal Properties. Figure 3 shows the phonon dispersion curves along with symmetry lines in the Brillouin zone and the corresponding ε-Ga_2O_3 phonon DOS. There are 120 phonon modes that span frequencies up to a maximum value of 21.9 THz at the Γ point. The diagonal Born effective charges are Ga_1 = (2.92, 2.93, 3.06), Ga_2 = (3.51, 3.29, 2.88), Ga_3 = (3.35, 3.20, 3.49), Ga_4 = (3.35, 3.45, 3.22), O_1 = (−2.49, −2.12, −2.31), O_2 = (−2.11, −2.30, −2.13), O_3 = (−2.13, −2.15, −1.93), O_4 = (−1.98, −2.06, −2.53), O_5 = (−2.17, −2.14, −1.96), and O_6 = (−2.24, −2.10, −1.76) in units of electron charge. The off-diagonal components are below 0.3, and none of them are reported. The high-frequency dielectric tensor of ε-Ga_2O_3 is somewhat isotropic with $\epsilon_{\infty_{11}} = 4.4$, $\epsilon_{\infty_{22}} = 4.3$, and $\epsilon_{\infty_{33}} = 4.3$. The dielectric tensor calculated by DPFT is consistent with the quasi-particle calculation result with $\varepsilon_\infty = 4.3$ solved by the Bethe−Salpeter equation of many-body perturbation theory.[4] The dielectric constant of ε-Ga_2O_3 is slightly greater than that of β-Ga_2O_3 (see the Supporting Information Note III), demonstrating the dielectric functionality of ε-Ga_2O_3.

The ε-Ga_2O_3 thermal performance prediction is one of the key factors for rational acceleration of electronic devices, including the specific heat capacity at constant volume (C_V) and heat capacity at pressure (C_P), Debye temperature (Θ_D), speed of sound (v_s), mode-resolved Grüneisen ($\gamma(\mathbf{q}_j)$), average Grüneisen parameters (γ), thermal expansion coefficient (α_v), Debye temperature (Θ_D), and lattice thermal conductivity (κ_L).[19] The phonon dispersion is essential to determine other thermal properties of a material such as the heat capacity. The heat capacity C_V is shown as a green solid line in Figure 4a. The Dulong−Petit limit of 3R is plotted as a black dashed line in Figure 4a, where R is the gas constant. C_V reaches the Dulong−Petit limit at high temperatures, analogous to the case of β-Ga_2O_3.[20] Furthermore, if the ab initio-calculated C_V data were fitting to the Debye model, the Debye temperature Θ_D of ε-Ga_2O_3 could be predicted to be 673 K. For comparison, the Debye temperature of β-Ga_2O_3 was also estimated to be 685 K

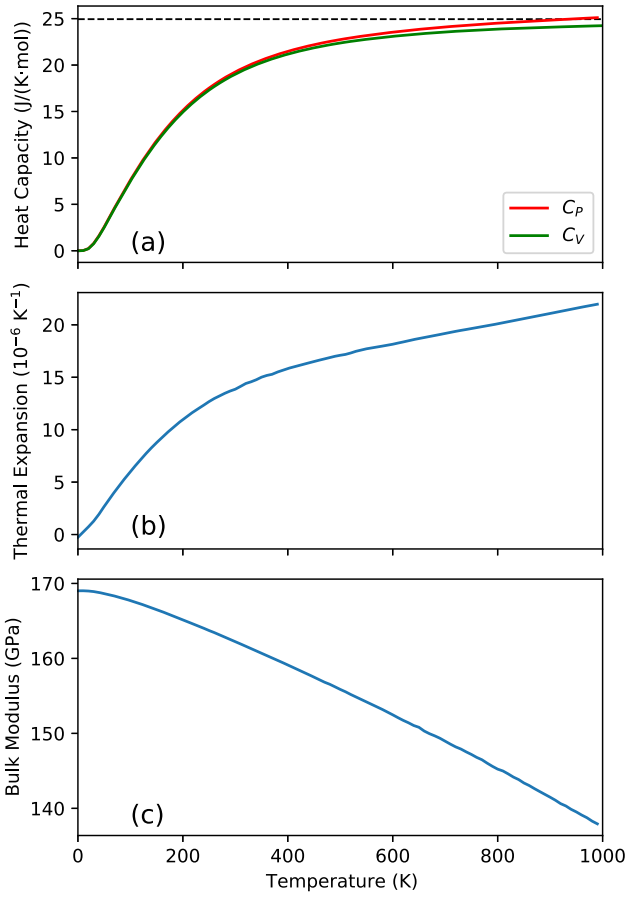

Figure 4. Thermal properties of ε-Ga_2O_3. (a) Heat capacity of ε-Ga_2O_3. Red and blue lines represent the heat capacity at constant pressure (C_P) and at constant volume (C_V), respectively. (b) Thermal expansion coefficient. (c) Bulk modulus.

in the same way (see Supporting Information Note IV and Figure S4), which was close to the experimental β-Ga_2O_3 Debye temperature of 738 K.[21] Therefore, the Debye temperature of ε-Ga_2O_3 predicted here is reasonable and is close to the Debye temperature of β-Ga_2O_3. The thermal expansion coefficient of ε-Ga_2O_3 is shown in Figure 4b. At room temperature, the thermal expansion coefficient is about

https://doi.org/10.1021/acsomega.1c06367
ACS Omega 2022, 7, 11643−11653

1.4×10^{-5} K^{-1}, which is higher than that of β-Ga_2O_3 (see Supporting Information Note IV.) The bulk modulus of ε-Ga_2O_3 is shown in Figure 4c. At room temperature, the bulk modulus of ε-Ga_2O_3 is about 162 GPa, which is also higher than that of β-Ga_2O_3 (see Supporting Information Note IV).

From the phonon dispersion near the Γ-point in Figure 3, it is clear that there are three branch acoustic phonons. The lower two branches (denoted as T_1 and T_2) belong to the transverse acoustic phonon, while the upper branch (denoted as L) belongs to the longitudinal acoustic phonon. In order to estimate the sound speed of ε-Ga_2O_3, the slopes of each acoustic branch are calculated near the Brillouin zone center along with three orthogonal directions by eq 19. The group velocities v_x, v_y, and v_z of acoustic phonon branch T_1, T_2, and L at each orthogonal direction x, y, and z are shown in Table 2.

Table 2. Group Velocities of ε-Ga_2O_3 Acoustic Phonons

acoustic phonon	v_x (km/s)	v_y (km/s)	v_z (km/s)	$\bar{v}$ (km/s)
T_1	3.0	3.4	2.8	3.1
T_2	4.1	3.6	3.5	3.7
L	7.4	6.3	7.1	7.0
v_s	5.2	4.6	4.8	4.9

The group velocity at each acoustic branch is defined as the average of the square

$$\bar{v} = \sqrt{\frac{1}{3}(v_x^2 + v_y^2 + v_z^2)} \tag{4}$$

Two transverse sound speeds v_{T_1} and v_{T_2} and one longitudinal sound speed v_L are 3.1, 3.7, and 7.0 km/s, respectively. The speed of sound is further estimated by the average of the transverse and longitudinal sound speed using

$$v_s = \sqrt{\frac{1}{3}(v_{T_1}^2 + v_{T_2}^2 + v_L^2)} \tag{5}$$

Afterward, the sound speed of ε-Ga_2O_3 is v_s = 4.9 km/s, which is slightly smaller than the sound speed of β-Ga_2O_3 (see the Supporting Information Note IV). Besides, the sound speeds at the three orthogonal directions are 5.2, 4.6, and 4.8 km/s, respectively.

The frequency-dependent mode Grüneisen parameters of ε-Ga_2O_3 by the Phonopy software package are shown in Figure 5. The **q** mesh is set to 20 × 20 × 20. The colors of the mode Grüneinen parameters are set for band indices with ascending order of phonon frequencies, which is indicated by the color bar in Figure 5. The Grüneisen parameters of the acoustic modes are mostly positive. A negative Grüneisen parameter indicates an increase in phonon frequency with increasing volume. An average Grüneisen parameter, $\gamma(T)$, can be obtained using

$$\gamma(T) = \frac{\sum_{\mathbf{q}j} \gamma_{\mathbf{q}j} C_{V_{\mathbf{q}j}}}{C_V} \tag{6}$$

where $C_{V_{\mathbf{q}_j}}$ are the mode contributions to the heat capacity. Using eq 6, we found that the average Grüneisen parameter of ε-Ga_2O_3 is 1.4 at 300 K. A simple phenomenological expression for the lattice thermal conductivity due to phonon−phonon scattering has been given by Slack and Morelli[22,23]

$$\kappa_L = A\frac{\bar{M}\Theta_D^3\delta}{\gamma^2 n^{2/3} T} \tag{7}$$

where κ_L is the lattice thermal conductivity, $\bar{M}$ is the average atomic mass, n is the number of atoms per unit cell, δ^3 is the volume per atom, T is the temperature, γ is the average Grüneisen parameter for the acoustic branches, and Θ_D is the Debye temperature. A is a Grüneisen parameter-dependent quantity equal to

$$A = \frac{2.43 \times 10^6}{1 - \frac{0.514}{\gamma} + \frac{0.228}{\gamma^2}} \tag{8}$$

if the temperature is in Kelvin, δ is in Angstroms, and the mass is in atomic units, κ_L is in W/(m·K). This phenomenological expression in eq 7 has been widely used for materials with different crystal structures and with thermal conductivities extending over several orders of magnitude.[23] The lattice thermal conductivity of ε-Ga_2O_3 calculated by eq 7 is shown in Figure 6. The thermal conductivity of ε-Ga_2O_3 is estimated to be 12 W/(m·K) at room temperature by eq 7, which is about 29% of the β-Ga_2O_3 thermal conductivity (see Supporting Information Note IV). There are two reasons for the lower thermal conductivity of ε-Ga_2O_3 than β-Ga_2O_3. First, the number of atoms in a unit cell of ε-Ga_2O_3 is two times that of

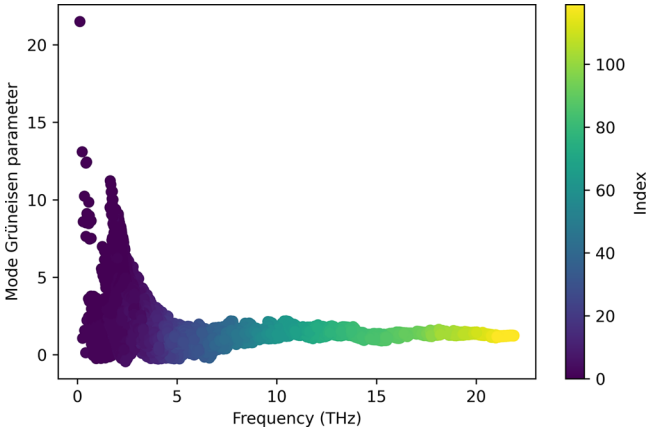

Figure 5. Frequency-dependent mode Grüneisen parameters.

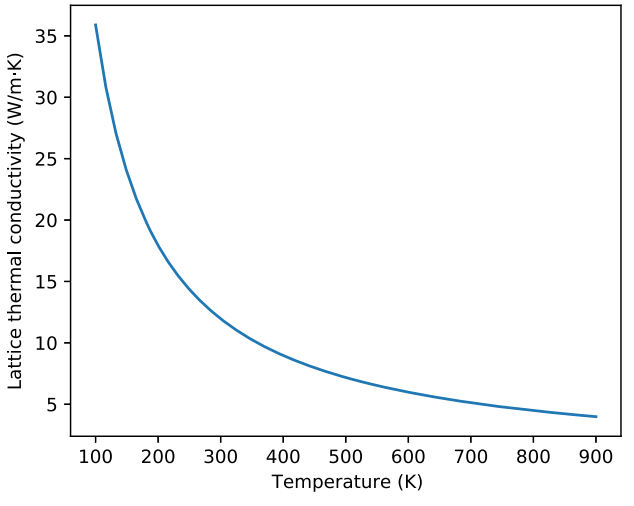

Figure 6. Lattice thermal conductivity as a function of temperature.

https://doi.org/10.1021/acsomega.1c06367
ACS Omega 2022, 7, 11643−11653

β-Ga_2O_3. Second, the Grüneisen parameter of ε-Ga_2O_3 is larger than that of β-Ga_2O_3. The mode Grüneisen parameter is an indicator of the anharmonic properties of materials.[24] Comparing the mode Grüneisen parameters of ε-Ga_2O_3 (see Figure 5) with those of β-Ga_2O_3 (see Supporting Information Figure S5), the mode Grüneisen parameters of an acoustic phonon in ε-Ga_2O_3 are much larger than those of β-Ga_2O_3. Therefore, the lower thermal conductivity of ε-Ga_2O_3 can be due to the anharmonic properties of an acoustic phonon of ε-Ga_2O_3. If we assume that all phonon relaxation times are the same, the thermal conductivity along with three orthogonal directions i can be proportional to the square of the sound speed v_{s_i}[21]

$$\kappa_i \propto v_{s_i}^2 \tag{9}$$

where $i = x, y, z$. Using the results in Table 2, the anisotropy of thermal conductivity can be obtained, $\kappa_x = 1.12\kappa_L$, $\kappa_y = 0.90\kappa_L$, and $\kappa_z = 0.98\kappa_L$. The thermal conductivity anisotropy of ε-Ga_2O_3 is smaller than that of ε-Ga_2O_3. It is worth mentioning that this phenomenological model does not take into account the effect of doping and defects. Slomski et al. already indicated that a moderate doping level of β-Ga_2O_3 does not change the thermal conductivity appreciably.[25] Oxygen vacancy is the most common point defect in Ga_2O_3.[26] Normally, the temperature-dependent thermal conductivity can be approximated by a simple power law $\kappa(T) \propto T^{-m}$. When other phonon scattering mechanisms are considered, the slope m will differ from 1. The point defects in Ga_2O_3 can provide an additional term for the thermal resistance which is proportional to the temperature and unrelated to the phonon−phonon scattering.[27] Therefore, the point defects can reduce the thermal conductivity of ε-Ga_2O_3, which can cause the heat dissipation problem in ε-Ga_2O_3-based electronic devices.

2.3. Thermoelectric Properties. A detailed understanding of the electrical transport and energy dissipation phenomena is crucial for the development of high-performance electronic materials for application. In the past, the thermal and electrical transport properties of ε-Ga_2O_3 have been studied in detail. Although there have been many detailed studies on the thermal and electrical transport properties of β-Ga_2O_3 in the past,[28,29] few systematic works have been reported on the thermoelectric coefficients of ε-Ga_2O_3 over a wide range of doping concentrations and temperatures. It is clear that the most challenging computational task is the determination of the band velocities $v_i(n, \mathbf{k})$ from an ab initio perspective. To treat doping of ε-Ga_2O_3 in the transport calculation, one of the simplest approaches is the rigid band approximation.[30] The band structure will be assumed to remain unchanged as the Fermi level moves up and down to simulate electron doping. To fill this gap, we systematically computed the corresponding Seebeck coefficient S, electrical conductivity σ, and power factor as a function of doping concentrations at various values of the chemical potential φ.

The electron relaxation time is an important parameter to determine the electron transport properties under a constant relaxation time approximation. Similar to GaN and GaAs, a polar optical phonon (POP) plays a vital role in the electron scattering of ε-Ga_2O_3 because of the strong ionic Ga−O bonding.[32−34] Therefore, both acoustic phonon scattering and polar optical phonon scattering were considered in the electron relaxation time calculation. First, the electron relaxation time will be calculated by eq 27. The material parameters for calculation of the electron relaxation time of ε-Ga_2O_3 are shown in Table 3. The mass density of ε-Ga_2O_3 is based on the experimental lattice constant.[35] The deformation potential of ε-Ga_2O_3 is about 12.6 eV as calculated by eq 28, and it is a little higher than the value of β-Ga_2O_3. The polar phonon energy in Table 3 is estimated from the average of all of the longitudinal optical phonon energies at all three Cartesian directions. The polar phonon energy of ε-Ga_2O_3 is about 47.2 meV, which is slightly smaller than the value of β-Ga_2O_3 (see Supporting Information Note V and Table S3). The electron relaxation times due to both acoustic phonon and polar optical phonon scattering are plotted in Figure 7. The polar optical phonon scattering is always larger than that of the acoustic phonon when the temperature is larger than about 100 K. In particular, when the temperature is above room temperature, the acoustic phonon scattering in ε-Ga_2O_3 can be neglected. The electron relaxation time at room temperature is about 15.1 fs, which is smaller than that of β-Ga_2O_3 (Supporting Information Note V and Figure S6). The calculated Seebeck coefficient of ε-Ga_2O_3 versus carrier concentration (N) and temperature (T) are shown in Figure 8a. The absolute value of the Seebeck coefficient is evidently decreasing with increasing carrier concentration. Furthermore, the Seebeck coefficient decreases almost linearly with increasing $\log(N_D)$. The electrical conductivity of ε-Ga_2O_3 is shown in Figure 8b, which increases with the doping concentration. It can be seen that for a given temperature the electric conductivity of ε-Ga_2O_3 has the highest value when the value of φ is close to the bottom of the conduction band minimum. The electronic thermal conductivity of ε-Ga_2O_3 is shown in Figure 8c, which increases with both the carrier concentration and temperature. The electronic thermal conductivity is much lower compared

Table 3. Material Parameters of β-Ga_2O_3 for Electron Relaxation Time Calculations

parameter	symbol	value
electron effective mass (m_e)	m^*	0.217
deformation potential (eV)	D	12.6
polar phonon energy (meV)	$\hbar\omega_{LO}$	47.2
mass density (kg/m^3)	ρ	5.9×10^3
static frequency dielectric constant[31]	ε_s	13.2
high-frequency dielectric constant	ε_∞	4.3
sound velocity (m/s)	v_s	4.9×10^3

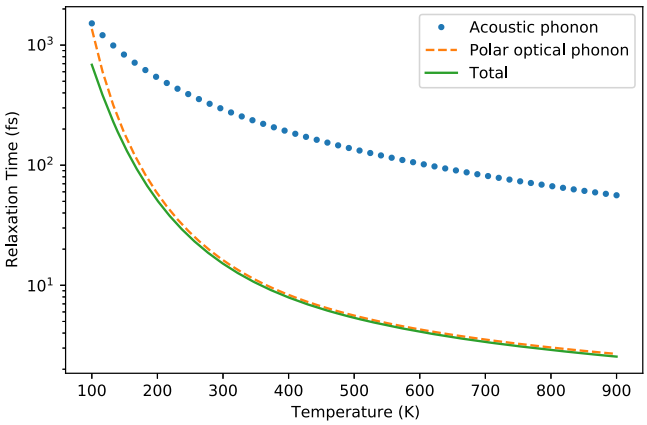

Figure 7. Relaxation time of ε-Ga_2O_3.

https://doi.org/10.1021/acsomega.1c06367
ACS Omega 2022, 7, 11643−11653

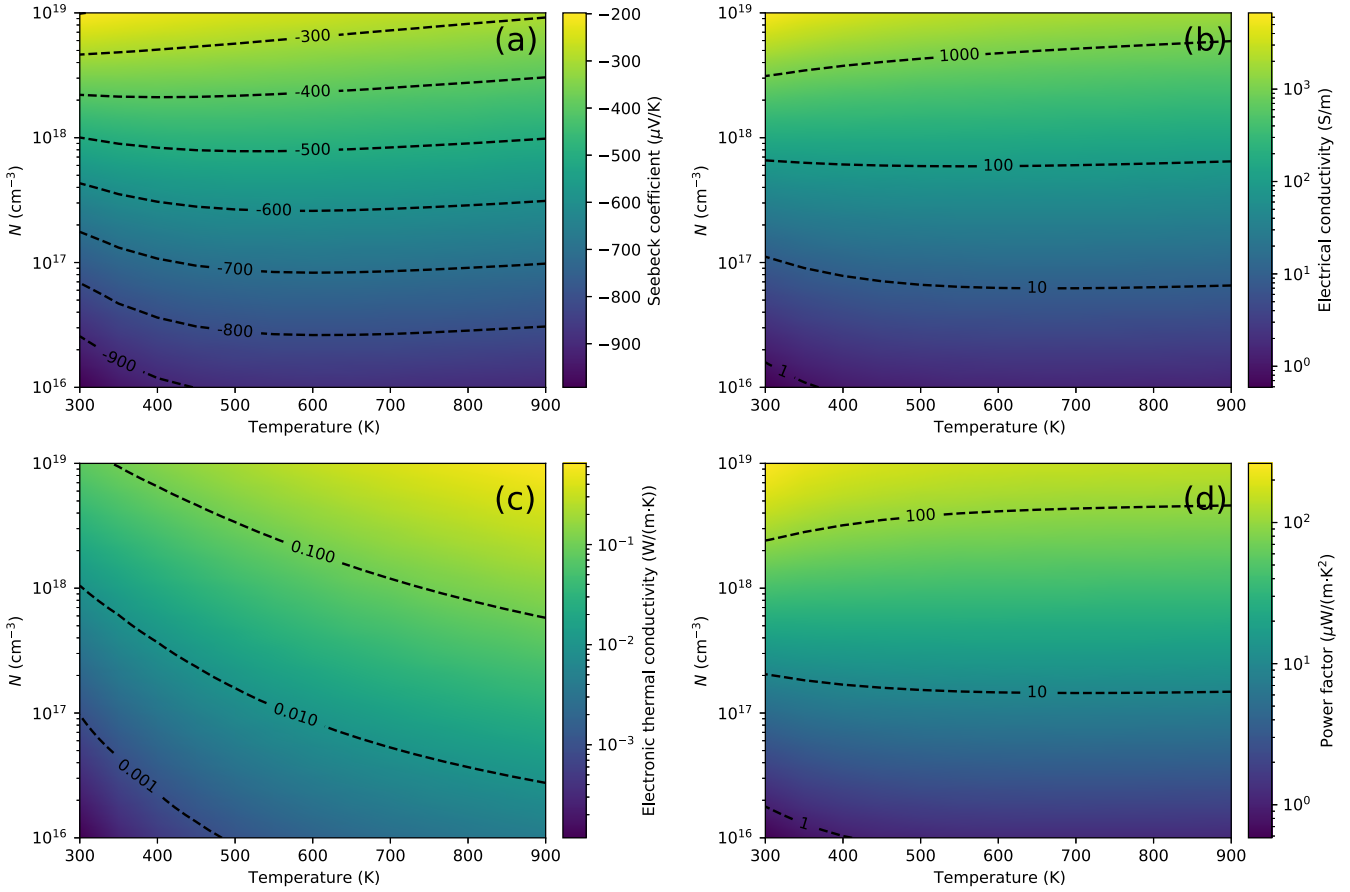

Figure 8. Thermoelectric properties of ε-Ga_2O_3 versus carrier concentration (n) on a logarithmic scale and temperature from 300 to 900 K: (a) Seebeck coefficient, (b) electrical conductivity (on a logarithmic scale), (c) electronic thermal conductibility (on a logarithmic scale), and (d) power factor (on a logarithmic scale).

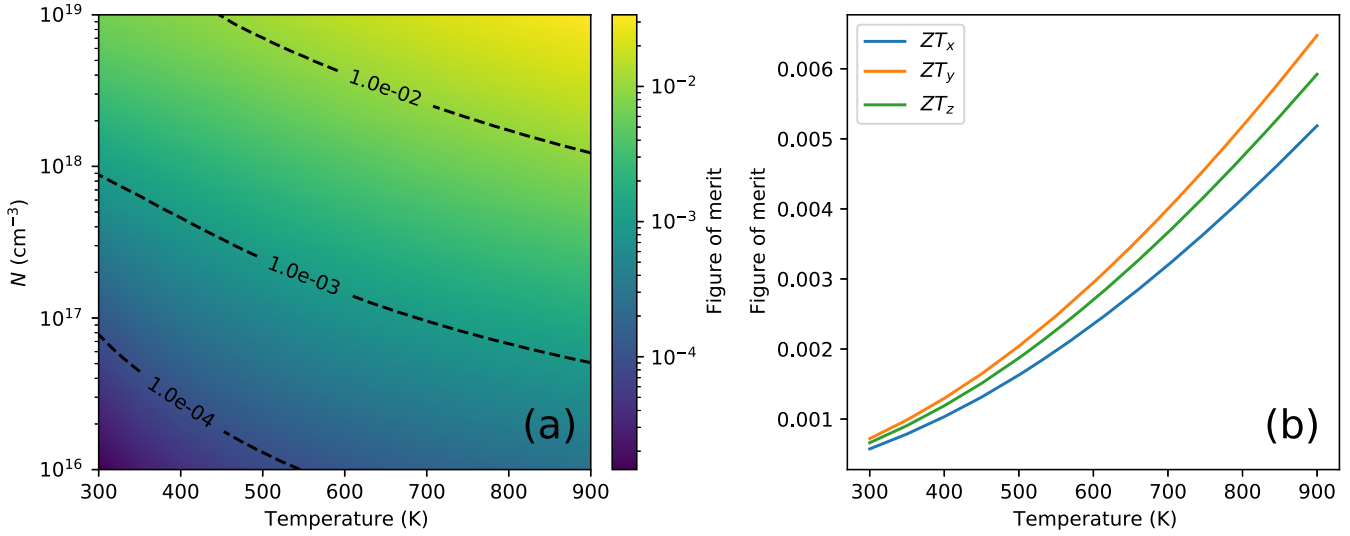

Figure 9. (a) Average figure of merit of ε-Ga_2O_3 (on logarithmic scale). (b) Figure of merit at the Cartesian directions when $N = 5.5 \times 10^{17}$ cm^{-3}.

to the lattice thermal conductivity shown in Figure 6. The power factor of a thermoelectric material is given by

$$P = \sigma S^2 \tag{10}$$

where S is the Seebeck coefficient and σ is the electrical conductivity. The power factor involves all of the important electrical properties of the material. Figure 8d shows the power factor of ε-Ga_2O_3, which indicates that the power factor increases with increasing doping concentration.

Although the Seebeck coefficient decreases as the doping concentration increases, the power factor of ε-Ga_2O_3 still increases with increasing doping concentration as the electrical conductivity increases more with increasing doping concentration. To date, no measured Seebeck coefficient of ε-Ga_2O_3

https://doi.org/10.1021/acsomega.1c06367
ACS Omega 2022, 7, 11643−11653

can be found in the literature. The Seebeck coefficient of β-Ga_2O_3 has been reported to be $-(300 \pm 20)$ μV/K with a 5.5 $\times$ 10^{17} cm^{-3} carrier concentration.[28] Our calculated Seebeck coefficient of β-Ga_2O_3 is 373 μV/K with a 5.5 $\times$ 10^{17} cm^{-3} carrier concentration (for more details see Supporting Information Note V and Figure S7), while the calculated Seebeck coefficient of ε-Ga_2O_3 is 572 μV/K with a 5.5 $\times$ 10^{17} cm^{-3} carrier concentration. Compared with β-Ga_2O_3, the Seebeck coefficient of ε-Ga_2O_3 is nearly 1.5 times larger at room temperature, when the carrier concentration of both phases of Ga_2O_3 is the same. However, because of its lower electrical conductivity, the power factor of ε-Ga_2O_3 is only 18% of β-Ga_2O_3 when the carrier concentration is 5.5 $\times$ 10^{17} cm^{-3} (see Supporting Information Note V). Furthermore, the electrical conductivity and the Seebeck coefficient are quite isotropic. The anisotropy of the electrical conductivity and the Seebeck coefficient at the Cartesian directions is less than 1% and 0.1%, respectively.

The validity of a material for thermoelectric applications depends on a dimensionless parameter, figure of merit, which can be described by[36]

$$ZT = \frac{\sigma S^2 T}{\kappa} \tag{11}$$

where S is the Seebeck coefficient, σ is the electrical conductivity, T is the absolute temperature, and κ is the thermal conductivity. Since $\kappa = \kappa_L + \kappa_e$ and κ_L is much higher than κ_e, $\kappa \approx \kappa_L$. Then, the figure of merit of ε-Ga_2O_3 can be further obtained from previous calculated results, which is shown in Figure 9a. When the carrier concentration is 5.5 $\times$ 10^{17} cm^{-3}, the figure of merit of ε-Ga_2O_3 is about 6.4 $\times$ 10^{-4} at room temperature, which is about 36% lower than the value of β-Ga_2O_3 (see Supporting Information Note V). The main reasons are that (1) the Seebeck coefficient of ε-Ga_2O_3 is higher than that of β-Ga_2O_3 and the lattice thermal conductivity of ε-Ga_2O_3 is lower than that of β-Ga_2O_3 when the concentration ranges from 1 $\times$ 10^{16} to 1 $\times$ 10^{19} cm^{-3} at room temperature and (2) the electrical conductivity of ε-Ga_2O_3 increases more rapidly as the carrier concentration increases at room temperature. Therefore, the figure of merit of ε-Ga_2O_3 can increase by increasing the doping concentration. Figure 9b shows the figure of merit at the Cartesian directions, which is expressed using a function of temperature, when the concentration is about 5.5 $\times$ 10^{17} cm^{-3}. Figure 9b indicates that the figure of merit at the y direction is always largest among the Cartesian directions. The main reason is that the electrical conductivity and the Seebeck coefficient are nearly the same at all Cartesian directions due to the isotropic band structure near the conduction band maximum. Therefore, the anisotropy of the figure of merit is determined by the anisotropy of the lattice thermal conductivity.

3. CONCLUSION

In conclusion, we obtained a suitable description using ab initio calculation for the electronic structure of ε-Ga_2O_3. The phonon dispersion and thermal properties of ε-Ga_2O_3 were obtained by density perturbation functional theory, the finite displacement method, and the quasi-harmonic approximation method. In the study of the ε-Ga_2O_3 transport properties, the band structure was first interpolated by a maximally localized Wannier function. Then, the results of the ab initio band energies were integrated with the semiclassical Boltzmann transport theory. This study shows that an appropriate description of the band structure together with phonon dispersion facilitates the study of the transport and thermoelectric properties of ε-Ga_2O_3. The thermoelectric coefficients of ε-Ga_2O_3 have been investigated systematically and provide predictive data. The electronic, thermal and thermoelectric properties of ε-Ga_2O_3 are compared with those of β-Ga_2O_3. The results reveal that (1) the effective mass, dielectric tensor, heat capacity, average Grüneisen parameter, and thermal conductivity of both ε-Ga_2O_3 and β-Ga_2O_3 can be comparable, (2) the Seebeck coefficient of ε-Ga_2O_3 is larger than that of β-Ga_2O_3, but the electrical conductivity of ε-Ga_2O_3 is smaller than that of β-Ga_2O_3, and (3) the thermoelectric figure of merit of ε-Ga_2O_3 increases as the carrier concentration increases. Our estimated temperature and concentration dependence of the electrical conductivity, Seebeck coefficient, and figure of merit give guidelines for the thermal management and design of ε-Ga_2O_3-based electronic devices.

COMPUTATIONAL METHODS

Density Functional Theory Calculation. The Quantum ESPRESSO package is used for all density generalized function theory (DFT) calculations.[37,38] A plane-wave basis set and the projector augmented-wave (PAW) method are used with the Perdew–Burke–Ernzerhof (PBE) exchange-correlation functional.[39,40] All the pseudopotentials are taken from SSSP pseudopotential library[41] and pslibrary.[42] Ga $3d^{10}$ $4s^2$ $4p^1$ and O $2s^2$ $2p^4$ are treated as the valence states. The system energy convergence criterion is set as 1 $\times$ 10^{-9} eV. The plane-wave self-consistence field calculation converges with a plane-wave cutoff of 70 Ry and a 7 $\times$ 4 $\times$ 4 Brillouin zone grid.[43] Optimization of the structure is truncated after the Hellmann–Feynman force up to 3 $\times$ 10^{-4} eV/Å. Afterward, the details of the ε-Ga_2O_3 band structure are obtained by maximally localized Wannier functions (MLWFs).[44,45] The SeeK-path tool was used to define the **k**-point and **q**-point labels.[46] The dielectric constant and Born effective charge are calculated by the PHonon package using density functional perturbation theory (DFPT) with only the Γ-**q**-point.[37,38,47,48]

Finite Displacement Method. Under the harmonic approximation, the atoms are assumed to move around their equilibrium positions $\mathbf{r}_l$, where l is the label of atoms in each unit cell. In the finite displacement method,[49,50] the approximation of the equation for the second-order force constant can be expressed as

$$\Phi_{\alpha\beta,l,l} \simeq -\frac{F_{\beta,l,}(\Delta \mathbf{r}_{\alpha,l})}{\Delta \mathbf{r}_{\alpha,l}} \tag{12}$$

where α and β are the Cartesian indices, l and l' are the indices of atoms in a unit cell, $\Delta \mathbf{r}_{\alpha,l}$ is the finite displacement of atoms l at α Cartesian index, and $F_{\beta,l'}(\Delta \mathbf{r}_{\alpha,l})$ is the force of atom l' at β Cartesian index due to $\Delta \mathbf{r}_{\alpha,l}$. The atomic force can be obtained from first principles by Quantum ESPRESSO. After the second-order force constant is calculated, the dynamical matrix $\mathbf{D}_{\alpha\beta,l'l}$ can be further calculated as long as the phonon dispersion $\omega(\mathbf{q}_j)$. All of the harmonic phonon properties are obtained using Phonopy packages.[51] After we obtain the full relaxation structure of ε-Ga_2O_3, we generate a series of 2 $\times$ 2 $\times$ 1 ε-Ga_2O_3 supercells with atom displacement, resulting in a total 60 different supercells. The displacement length of each atom from its equilibrium position is 0.01 Å. All of the supercells contain in total 160 atoms. Then, the ground state

https://doi.org/10.1021/acsomega.1c06367
ACS Omega 2022, 7, 11643−11653

energies of these 60 supercells are calculated by Quantum ESPRESSO. After the energies of these supercells are obtained, the force constant can be calculated by Phonopy. From the force constant we could further calculate the phonon band structure and the phonon density of states. The phonon dispersion is further interpolated with nonanalytical term correction.[47,52−54] Once the phonon band structure is obtained, the phonon mode contribution to the harmonic phonon energy can be calculated as

$$E_{\mathbf{q}_j} = \hbar\omega_{\mathbf{q}_j}\left[\frac{1}{2} + \frac{1}{\exp(\hbar\omega(\mathbf{q}_j)/k_B T) - 1}\right] \tag{13}$$

where j is the phonon band index and ω is the phonon frequency. Then, we can express the total phonon energy as follows

$$E = \sum_{\mathbf{q}_j} E_{\mathbf{q}_j} \tag{14}$$

On the other hand, the Helmholtz free energy can be expressed as

$$H_{\text{phonon}} = \sum_{\mathbf{q}_j}\left\{\frac{1}{2}\hbar\omega_{\mathbf{q}_j} + k_B T \ln\left[1 - \exp\left(-\frac{\hbar\omega_{\mathbf{q}_j}}{k_B T}\right)\right]\right\} \tag{15}$$

Afterward, the constant volume heat capacity C_V can be calculated as

$$C_V = \left(\frac{\partial E}{\partial T}\right)_V = \sum_{\mathbf{q}_j}\left(\frac{\partial E_{\mathbf{q}_j}}{\partial T}\right)_V = \sum_{\mathbf{q}_j} C_{V_{\mathbf{q}_j}} \tag{16}$$

where $C_{V_{\mathbf{q}_j}}$ is mode contributions to the heat capacity, which is defined by

$$C_{V_{\mathbf{q}j}} = k_B\left(\frac{\hbar\omega_{\mathbf{q}j}}{k_B T}\right)^2 \frac{\exp\left(\frac{\hbar\omega_{\mathbf{q}j}}{k_B T}\right)}{\left[\exp\left(\frac{\hbar\omega_{\mathbf{q}j}}{k_B T}\right) - 1\right]^2} \tag{17}$$

Thereby, the heat capacity at constant volume C_V can be obtained directly as the second derivative of the Helmholtz free energy with respect to temperature. According to the Debye model, the heat capacity at constant volume $C_V(T)$ as function of temperature can be approximated by

$$C_V(T) = 9Nk_B\left(\frac{T}{\Theta_D}\right)^3 \int_0^{T/\Theta_D} \frac{x^4 e^x}{(e^x - 1)^2} dx \tag{18}$$

If $C_V(T)$ is calculated by eq 16 with a temperature step of 10 K, which is used to fit eq 18 by the Python package Lmfit, the Debye temperature Θ_D can be obtained. Besides, when the phonon dispersion is acquired, the group velocity $\mathbf{v}_g$ can be calculated by the finite difference method as follows

$$\mathbf{v}_g = \frac{\partial\omega_{\mathbf{q}_j}}{\partial\mathbf{q}} \approx \frac{\Delta\omega_{\mathbf{q}_j}}{\Delta\mathbf{q}} \tag{19}$$

where $\mathbf{q}$ is the phonon vector and j is the phonon band index. Because the acoustic phonon dispersion at the Γ point is divergent, the group velocity of an acoustic phonon at the Γ point will be approximated by the points slightly away from the center in the different directions, i.e., v_x, v_y, and v_z, where x, y, and z are the Cartesian directions. The sound speed will be further approximated by the average of the square root of the group velocity along the three orthogonal directions.

Quasi-Harmonic Approximation. The thermal properties at constant pressure are further obtained by a quasi-harmonic approximation,[55] in which we need to calculate the Gibbs free energy, which is defined as follows

$$G(T, p) = \min_V [U_{\text{electron}}(V) + H_{\text{phonon}}(T, V) + pV] \tag{20}$$

where V is the volume, p is the pressure, $U_{\text{electron}}(V)$ is the total energy of the electronic structure with different volumes, and $H_{\text{phonon}}(T, V)$ is the Helmholtz free energy with different temperatures and different volumes. In this work, 9 volume points are used with a temperature step of 10 K, and the lattice constant step is 0.025 Å. After we calculate the Helmholtz free energy with different temperatures and volumes using eq 15, we could further obtain the Gibbs free energy at the temperature and the respective equilibrium volume $V(T)$. The volume thermal expansion coefficient can be acquired from the equilibrium volume as

$$\beta(T) = \frac{1}{V(T)}\frac{\partial V(T)}{\partial T} \tag{21}$$

The heat capacity at constant pressure C_p is given by

$$C_p = -T\frac{\partial^2 G(T, p)}{\partial T^2} \tag{22}$$

Furthermore, the equilibrium volume $V(T)$ is used to fit the Vinet equation of state, which is described by[56]

$$p = 3B_0\left(\frac{1-\eta}{\eta^2}\right)\exp\left[\frac{3}{2}(B_0' - 1)(1 - \eta)\right] \tag{23}$$

where B_0 is the isothermal bulk modulus and B_0' is the derivative of bulk modulus with respect to pressure. If the equilibrium volume at zero pressure is V_0, η is cube root of the specific volume, which is defined as

$$\eta = \left[\frac{V(T)}{V_0}\right]^{1/3} \tag{24}$$

(24)If the equilibrium volume $V(T)$ obtained from eq 20 is used to fit the equation of state in eq 23, the bulk modulus can be obtained. The mode Grüneisen parameter $\gamma(\mathbf{q}j)$ at the wave vector $\mathbf{q}$ and band index j is defined as[51]

$$\gamma(\mathbf{q}j) = -\frac{V}{\omega(\mathbf{q}j)}\frac{\partial\omega(\mathbf{q}j)}{\partial V} \tag{25}$$

where V is the volume and $\omega(\mathbf{q}_j)$ is the phonon frequency. It is easy to calculate $\gamma(\mathbf{q}_j)$ from the volume derivative of the dynamical matrix once the dynamical matrix $D(\mathbf{q})$ is acquired

$$\gamma(\mathbf{q}j) \approx -\frac{V}{2[\omega(\mathbf{q}j)]^2}\langle\mathbf{e}(\mathbf{q}j)|\frac{\Delta D(\mathbf{q})}{\Delta V}|\mathbf{e}(\mathbf{q}j)\rangle \tag{26}$$

where $\mathbf{e}(\mathbf{q}_j)$ is the eigenvector. The phonon dispersion is calculated at three different volumes to determine the Grüneisen parameters, one at the equilibrium volume and the other two at slightly distorted volumes (±0.5% lattice constant).

https://doi.org/10.1021/acsomega.1c06367
ACS Omega 2022, 7, 11643−11653

Boltzmann Transport Theory. The calculations of the thermoelectric and electronic transport are performed by Boltzmann transport theory within the constant relaxation time (τ) approximation implemented in the BoltzWann code.[44,45] The acoustic phonon scattering rate as a function of T is given by[34,57,58]

$$\frac{1}{\tau_{ac}(E, T)} = \frac{(2m^*)^{3/2} D^2 k_B T}{2\pi\hbar^4 \rho v_s^2} E^{1/2} \tag{27}$$

where m^* is the effective electron mass, k_B is the Boltzmann constant, T is the temperature, ρ is the mass density, v_s is the sound velocity, D is the deformation potential, and E is the electron energy. The deformation potential is calculated by[59,60]

$$D = \frac{\partial E_0}{\partial \ln V} \approx V_0 \frac{\Delta E_0}{\Delta V} \tag{28}$$

where E_0 is the conduction band minimum located at Γ and V_0 is the equilibrium unit cell volume. To obtain the absolute deformation potential of the conduction band minimum, the energy change is calculated as the difference between the conduction band minimum and a core level, e.g., the anion 2s core level, using a constant of 0.1% to expand and compress the lattice constant because the absolute position of the energy level is not well established in infinitely periodic crystals.[61] DFT calculation will be performed with several volumes by expanding and compressing the lattice constant by a step of 0.5%. The results of the energy and volume change will be fit to eq 27 by the Lmfit python package in order to obtain a better estimation of the deformation potential. On the other hand, the polar optical phonon scattering rate can be estimated by[32]

$$\frac{1}{\tau_{pop}} = \frac{e^2 \omega_{LO}}{2\sqrt{2}\pi\epsilon_0\hbar}\left(\frac{1}{\epsilon_\infty} - \frac{1}{\epsilon_s}\right)\frac{\sqrt{m^*}}{\sqrt{E}} \times \left[(n_q + 1)\sinh^{-1}\sqrt{\frac{E - \hbar\omega_{LO}}{\hbar\omega_{LO}}} + n_q \sinh^{-1}\sqrt{\frac{E}{\hbar\omega_{LO}}}\right] \tag{29}$$

where ω_{LO} is the longitudinal optical phonon frequency, ε_0 is the vacuum permittivity, ε_∞ is the high-frequency dielectric constant, ε_s is the static dielectric constant, and n_q is Bose–Einstein distribution function for longitudinal optical phonons given by

$$n_q = \frac{1}{\exp(\hbar\omega_{LO}/k_B T) - 1} \tag{30}$$

We acquire the net relaxation rate using Matthiessen's rule

$$\frac{1}{\tau_{total}} = \frac{1}{\tau_{ac}} + \frac{1}{\tau_{pop}} \tag{31}$$

The average electron relaxation time is given by

$$\tau(T) = \frac{\langle \tau E \rangle}{\langle E \rangle} = \frac{\int_0^\infty \tau E^{3/2} f(E, T) dE}{\int_0^\infty E^{3/2} f(E, T) dE} \tag{32}$$

where $f(E, T)$ is the Fermi–Dirac distribution

$$f(E, T) = \frac{1}{\exp(E/k_B T) + 1} \tag{33}$$

The average electron relaxation time will be finally evaluated with numeric integration by SciPy.

On the basis of the Boltzmann transport equation, the following expressions are used to calculate the electrical conductivity $\boldsymbol{\sigma}$, electronic thermal conductivity $\boldsymbol{\kappa}_e$, and Seebeck coefficient $\mathbf{S}$ as a function of the chemical potential φ and of the temperature T

$$[\boldsymbol{\sigma}]_{ij}(\varphi, T) = e^2 \int_{-\infty}^{+\infty} dE \left(-\frac{\partial f(E, \varphi, T)}{\partial E}\right) \Sigma_{i,j}(E) \tag{34}$$

$$[\boldsymbol{\sigma}\mathbf{S}]_{ij}(\varphi, T) = \frac{e}{T} \int_{-\infty}^{+\infty} dE \left(-\frac{\partial f(E, \varphi, T)}{\partial E}\right)(E - \varphi) \Sigma_{i,j}(E) \tag{35}$$

$$[\boldsymbol{\kappa}_e]_{ij}(\varphi, T) = \frac{1}{T} \int_{-\infty}^{+\infty} dE \left(-\frac{\partial f(E, \varphi, T)}{\partial E}\right)(E - \varphi)^2 \Sigma_{i,j}(E) \tag{36}$$

Here, i and j are Cartesian indices, $\boldsymbol{\sigma}\mathbf{S}$ denotes the matrix product of the two tensors $\boldsymbol{\sigma}$ and $\mathbf{S}$, and $\partial f/\partial E$ is the derivative of the Fermi–Dirac distribution function with respect to the energy. Moreover, the transport distribution function $\Sigma_{ij}(E)$ is defined as

$$\Sigma_{ij}(E) = \frac{1}{V} \Sigma_{n,\mathbf{k}} v_i(n, \mathbf{k}) v_j(n, \mathbf{k}) \tau_{n\mathbf{k}} \delta(E - E_{n,\mathbf{k}}) \tag{37}$$

where the summation is over all bands n and over all of the Brillouin zone, $E_{n,\mathbf{k}}$ is the energy for band n at $\mathbf{k}$, τ_{nk} is the scattering time, and v_i is the ith component of the band velocity at $(n, \mathbf{k})$ which can be computed by

$$v_i(n, \mathbf{k}) = \frac{1}{\hbar}\frac{\partial E_{n,\mathbf{k}}}{\partial k_i} \tag{38}$$

Within the relaxation time approximation, τ_{nk} is held constant with respect to the electron on band n at wave vector $\mathbf{k}$; therefore, the Seebeck coefficient is independent of τ. This constant relaxation time approximation is based on the assumption that the variation of energy on the scale of $k_B T$ does not cause the electron scattering time to vary with it. This approximation is widely adopted in first-principles calculation for bulk materials.[30,36] BoltzWann code uses a maximally localized Wannier function (MLWF) set to interpolate the band structure obtained from first-principles calculations by Quantum ESPRESSO. First, a 8 × 4 × 4 $\mathbf{k}$-points grid is used for construction of 56 MLWFs around the gap region. Then, a 80 × 40 × 40 $\mathbf{k}$ mesh is utilized to calculate the transport properties. The band structure of the Wannier function interpolation matches well with the first-principles calculations of Quantum Espresso. In order to verify the computational methods, we also calculate the electronic, thermal, and thermoelectric properties of β-Ga_2O_3, which agree well with previous studies (see the Supporting Information).

■ ASSOCIATED CONTENT

Supporting Information

The Supporting Information is available free of charge at https://pubs.acs.org/doi/10.1021/acsomega.1c06367.

https://doi.org/10.1021/acsomega.1c06367
ACS Omega 2022, 7, 11643−11653

Electronic, thermal, and thermoelectric properties of β-Ga_2O_3 (PDF)

AUTHOR INFORMATION

Corresponding Author

Xianzhong Zhou − *School of Information Engineering, Guangdong University of Technology, 510006 Guangzhou, China*; orcid.org/0000-0003-4311-7287; Email: zhouxzh@gdut.edu.cn

Authors

Qingsong Liu − *School of Information Engineering, Guangdong University of Technology, 510006 Guangzhou, China*

Zimin Chen − *School of Electronics and Information Technology, Sun Yat-Sen University, 510275 Guangzhou, China*

Complete contact information is available at: https://pubs.acs.org/10.1021/acsomega.1c06367

Notes

The authors declare no competing financial interest.

ACKNOWLEDGMENTS

The authors are thankful for financial support from the Natural Science Foundation of China (Grant Nos. 61704032 and 61804187)

REFERENCES

(1) Higashiwaki, M.; Sasaki, K.; Murakami, H.; Kumagai, Y.; Koukitu, A.; Kuramata, A.; Masui, T.; Yamakoshi, S. Recent progress in Ga_2O_3 power devices. *Semicond. Sci. Technol.* **2016**, *31*, 034001.

(2) Singh Pratiyush, A.; Krishnamoorthy, S.; Vishnu Solanke, S.; Xia, Z.; Muralidharan, R.; Rajan, S.; Nath, D. N. High responsivity in molecular beam epitaxy grown β-Ga_2O_3 metal semiconductor metal solar blind deep-UV photodetector. *Appl. Phys. Lett.* **2017**, *110*, 221107.

(3) Kong, W.-Y.; Wu, G.-A.; Wang, K.-Y.; Zhang, T.-F.; Zou, Y.-F.; Wang, D.-D.; Luo, L.-B. Graphene-β-Ga_2O_3 Heterojunction for Highly Sensitive Deep UV Photodetector Application. *Adv. Mater.* **2016**, *28*, 10725−10731.

(4) Furthmüller, J.; Bechstedt, F. Quasiparticle bands and spectra of Ga_2O_3 polymorphs. *Phys. Rev. B* **2016**, *93*, 115204.

(5) Roy, R.; Hill, V. G.; Osborn, E. F. Polymorphism of Ga_2O_3 and the System Ga_2O_3—H_2O. *J. Am. Chem. Soc.* **1952**, *74*, 719−722.

(6) Yusa, H.; Tsuchiya, T.; Sata, N.; Ohishi, Y. Rh_2O_3(II)-type structures in Ga_2O_3 and In_2O_3 under high pressure: Experiment and theory. *Phys. Rev. B* **2008**, *77*, 064107.

(7) Oshima, Y.; Víllora, E. G.; Matsushita, Y.; Yamamoto, S.; Shimamura, K. Epitaxial growth of phase-pure ε-Ga_2O_3 by halide vapor phase epitaxy. *J. Appl. Phys.* **2015**, *118*, 085301.

(8) Nishinaka, H.; Tahara, D.; Yoshimoto, M. Heteroepitaxial growth of ε-Ga_2O_3 thin films on cubic (111) MgO and (111) yttria-stablized zirconia substrates by mist chemical vapor deposition. *Jpn. J. Appl. Phys.* **2016**, *55*, 1202BC.

(9) Xia, X.; Chen, Y.; Feng, Q.; Liang, H.; Tao, P.; Xu, M.; Du, G. Hexagonal phase-pure wide band gap ε-Ga_2O_3 films grown on 6H-SiC substrates by metal organic chemical vapor deposition. *Appl. Phys. Lett.* **2016**, *108*, 202103.

(10) Cora, I.; Mezzadri, F.; Boschi, F.; Bosi, M.; Čaplovičová, M.; Calestani, G.; Dódony, I.; Pécz, B.; Fornari, R. The real structure of ε-Ga_2O_3 and its relation to κ-phase. *CrystEngComm* **2017**, *19*, 1509−1516.

(11) Fornari, R.; Pavesi, M.; Montedoro, V.; Klimm, D.; Mezzadri, F.; Cora, I.; Pécz, B.; Boschi, F.; Parisini, A.; Baraldi, A.; Ferrari, C.; Gombia, E.; Bosi, M. Thermal stability of ε-Ga_2O_3 polymorph. *Acta Mater.* **2017**, *140*, 411−416.

(12) Yoshioka, S.; Hayashi, H.; Kuwabara, A.; Oba, F.; Matsunaga, K.; Tanaka, I. Structures and energetics of Ga_2O_3 polymorphs. *J. Phys.: Condens. Matter* **2007**, *19*, 346211.

(13) Pearton, S. J.; Yang, J.; Cary, P. H.; Ren, F.; Kim, J.; Tadjer, M. J.; Mastro, M. A. A review of Ga_2O_3 materials, processing, and devices. *Appl. Phys. Rev.* **2018**, *5*, 011301.

(14) Higashiwaki, M.; Sasaki, K.; Kuramata, A.; Masui, T.; Yamakoshi, S. Development of gallium oxide power devices. *Phys. Status Solidi A* **2014**, *211*, 21−26.

(15) Momma, K.; Izumi, F. *VESTA3* for three-dimensional visualization of crystal, volumetric and morphology data. *J. Appl. Crystallogr.* **2011**, *44*, 1272−1276.

(16) Yusa, S.; Oka, D.; Fukumura, T. High-κ dielectric ε-Ga_2O_3 stabilized in a transparent heteroepitaxial structure grown by mist CVD at atmospheric pressure. *CrystEngComm* **2020**, *22*, 381−385.

(17) Perdew, J. P.; Levy, M. Physical Content of the Exact Kohn-Sham Orbital Energies: Band Gaps and Derivative Discontinuities. *Phys. Rev. Lett.* **1983**, *51*, 1884−1887.

(18) Kittel, C. *Introduction to Solid State Physics*, 8th ed.; John Wiley & Sons, Inc.: New York, 2004.

(19) Nath, P.; Plata, J. J.; Usanmaz, D.; Orabi, R. A. R. A.; Fornari, M.; Nardelli, M. B.; Toher, C.; Curtarolo, S. High-throughput prediction of finite-temperature properties using the quasi-harmonic approximation. *Comput. Mater. Sci.* **2016**, *125*, 82−91.

(20) Mengle, K. A.; Kioupakis, E. Vibrational and electron-phonon coupling properties of β-Ga_2O_3 from first-principles calculations: Impact on the mobility and breakdown field. *AIP Adv.* **2019**, *9*, 015313.

(21) Guo, Z.; Verma, A.; Wu, X.; Sun, F.; Hickman, A.; Masui, T.; Kuramata, A.; Higashiwaki, M.; Jena, D.; Luo, T. Anisotropic thermal conductivity in single crystal β-gallium oxide. *Appl. Phys. Lett.* **2015**, *106*, 111909.

(22) Slack, G. A. *Solid State Physics*; Elsevier, 1979; pp 1−71.

(23) Morelli, D. T.; Slack, G. A. High Lattice Thermal Conductivity Solids. In *High Thermal Conductivity Materials*; Shindé, S. L.; Goela, J. S., Eds.; Springer-Verlag, 2006; pp 37−68.

(24) Porter, L. J.; Justo, J. F.; Yip, S. The importance of Grüneisen parameters in developing interatomic potentials. *J. Appl. Phys.* **1997**, *82*, 5378−5381.

(25) Slomski, M.; Blumenschein, N.; Paskov, P. P.; Muth, J. F.; Paskova, T. Anisotropic thermal conductivity of β-Ga_2O_3 at elevated temperatures: Effect of Sn and Fe dopants. *J. Appl. Phys.* **2017**, *121*, 235104.

(26) Dong, L.; Jia, R.; Xin, B.; Peng, B.; Zhang, Y. Effects of oxygen vacancies on the structural and optical properties of β-Ga_2O_3. *Sci. Rep.* **2017**, *7*, 40160.

(27) Callaway, J.; von Baeyer, H. C. Effect of Point Imperfections on Lattice Thermal Conductivity. *Phys. Rev.* **1960**, *120*, 1149−1154.

(28) Boy, J.; Handwerg, M.; Ahrling, R.; Mitdank, R.; Wagner, G.; Galazka, Z.; Fischer, S. F. Temperature dependence of the Seebeck coefficient of epitaxial β-Ga_2O_3 thin films. *APL Mater.* **2019**, *7*, 022526.

(29) Kumar, A.; Singisetti, U. First principles study of thermoelectric properties of β-gallium oxide. *Appl. Phys. Lett.* **2020**, *117*, 262104.

(30) Scheidemantel, T. J.; Ambrosch-Draxl, C.; Thonhauser, T.; Badding, J. V.; Sofo, J. O. Transport coefficients from first-principles calculations. *Phys. Rev. B* **2003**, *68*, 125210.

(31) Cho, S. B.; Mishra, R. Epitaxial engineering of polar ε-Ga_2O_3 for tunable two-dimensional electron gas at the heterointerface. *Appl. Phys. Lett.* **2018**, *112*, 162101.

(32) Ma, N.; Tanen, N.; Verma, A.; Guo, Z.; Luo, T.; Xing, H. G.; Jena, D. Intrinsic electron mobility limits in β-Ga_2O_3. *Appl. Phys. Lett.* **2016**, *109*, 212101.

(33) Ghosh, K.; Singisetti, U. Ab initio calculation of electron-phonon coupling in monoclinic β-Ga_2O_3 crystal. *Appl. Phys. Lett.* **2016**, *109*, 072102.

(34) Parisini, A.; Fornari, R. Analysis of the scattering mechanisms controlling electron mobility in β-Ga_2O_3 crystals. *Semicond. Sci. Technol.* **2016**, *31*, 035023.
(35) Liu, B.; Gu, M.; Liu, X. Lattice dynamical, dielectric, and thermodynamic properties of β-Ga_2O_3 from first principles. *Appl. Phys. Lett.* **2007**, *91*, 172102.
(36) Borges, P. D.; Scolfaro, L. Electronic and thermoelectric properties of InN studied using ab initio density functional theory and Boltzmann transport calculations. *J. Appl. Phys.* **2014**, *116*, 223706.
(37) Giannozzi, P.; et al. QUANTUM ESPRESSO: a modular and open-source software project for quantum simulations of materials. *J. Phys.: Condens. Matter* **2009**, *21*, 395502.
(38) Giannozzi, P.; et al. Advanced capabilities for materials modelling with Quantum ESPRESSO. *J. Phys.: Condens. Matter* **2017**, *29*, 465901.
(39) Perdew, J. P.; Burke, K.; Ernzerhof, M. Generalized Gradient Approximation Made Simple. *Phys. Rev. Lett.* **1996**, *77*, 3865−3868.
(40) Kresse, G.; Joubert, D. From ultrasoft pseudopotentials to the projector augmented-wave method. *Phys. Rev. B* **1999**, *59*, 1758−1775.
(41) Prandini, G.; Marrazzo, A.; Castelli, I. E.; Mounet, N.; Marzari, N. Precision and efficiency in solid-state pseudopotential calculations. *npj Comput. Mater.* **2018**, *4*, 72.
(42) Dal Corso, A. Pseudopotentials periodic table: From H to Pu. *Comput. Mater. Sci.* **2014**, *95*, 337−350.
(43) Monkhorst, H. J.; Pack, J. D. Special points for Brillouin-zone integrations. *Phys. Rev. B* **1976**, *13*, 5188−5192.
(44) Pizzi, G.; Volja, D.; Kozinsky, B.; Fornari, M.; Marzari, N. BoltzWann: A code for the evaluation of thermoelectric and electronic transport properties with a maximally-localized Wannier functions basis. *Comput. Phys. Commun.* **2014**, *185*, 422−429.
(45) Pizzi, G.; Volja, D.; Kozinsky, B.; Fornari, M.; Marzari, N. An updated version of BoltzWann: A code for the evaluation of thermoelectric and electronic transport properties with a maximally-localized Wannier functions basis. *Comput. Phys. Commun.* **2014**, *185*, 2311−2312.
(46) Hinuma, Y.; Pizzi, G.; Kumagai, Y.; Oba, F.; Tanaka, I. Band structure diagram paths based on crystallography. *Comput. Mater. Sci.* **2017**, *128*, 140−184.
(47) Gonze, X.; Lee, C. Dynamical matrices, Born effective charges, dielectric permittivity tensors, and interatomic force constants from density-functional perturbation theory. *Phys. Rev. B* **1997**, *55*, 10355−10368.
(48) Baroni, S.; de Gironcoli, S.; Dal Corso, A.; Giannozzi, P. Phonons and related crystal properties from density-functional perturbation theory. *Rev. Mod. Phys.* **2001**, *73*, 515−562.
(49) Chaput, L.; Togo, A.; Tanaka, I.; Hug, G. Phonon-phonon interactions in transition metals. *Phys. Rev. B* **2011**, *84*, 094302.
(50) Parlinski, K.; Li, Z. Q.; Kawazoe, Y. First-Principles Determination of the Soft Mode in Cubic ZrO_2. *Phys. Rev. Lett.* **1997**, *78*, 4063−4066.
(51) Togo, A.; Tanaka, I. First principles phonon calculations in materials science. *Scr. Mater.* **2015**, *108*, 1−5.
(52) Pick, R. M.; Cohen, M. H.; Martin, R. M. Microscopic Theory of Force Constants in the Adiabatic Approximation. *Phys. Rev. B* **1970**, *1*, 910−920.
(53) Gonze, X.; Charlier, J.-C.; Allan, D.; Teter, M. Interatomic force constants from first principles: The case of α-quartz. *Phys. Rev. B* **1994**, *50*, 13035−13038.
(54) Wang, Y.; Wang, J. J.; Wang, W. Y.; Mei, Z. G.; Shang, S. L.; Chen, L. Q.; Liu, Z. K. A mixed-space approach to first-principles calculations of phonon frequencies for polar materials. *J. Phys.: Condens. Matter* **2010**, *22*, 202201.
(55) Togo, A.; Chaput, L.; Tanaka, I.; Hug, G. First-principles phonon calculations of thermal expansion in Ti_3SiC_2, Ti_3AlC_2 and Ti_3GeC_2. *Phys. Rev. B* **2010**, *81*, 174301.
(56) Vinet, P.; Smith, J. R.; Ferrante, J.; Rose, J. H. Temperature effects on the universal equation of state of solids. *Phys. Rev. B* **1987**, *35*, 1945−1953.
(57) Bardeen, J.; Shockley, W. Deformation Potentials and Mobilities in Non-Polar Crystals. *Phys. Rev.* **1950**, *80*, 72−80.
(58) Hu, Y.; Hwang, J.; Lee, Y.; Conlin, P.; Schlom, D. G.; Datta, S.; Cho, K. First principles calculations of intrinsic mobilities in tin-based oxide semiconductors SnO, SnO2, and Ta2SnO6. *J. Appl. Phys.* **2019**, *126*, 185701.
(59) Qiao, J.; Kong, X.; Hu, Z.-X.; Yang, F.; Ji, W. High-mobility transport anisotropy and linear dichroism in few-layer black phosphorus. *Nat. Commun.* **2014**, *5*, 4475.
(60) Dong, B.; Wang, Z.; Hung, N. T.; Oganov, A. R.; Yang, T.; Saito, R.; Zhang, Z. New two-dimensional phase of tin chalcogenides: Candidates for high-performance thermoelectric materials. *Physical Review Materials* **2019**, *3*, 013405.
(61) Li, Y.-H.; Gong, X. G.; Wei, S.-H. Ab initio calculation of hydrostatic absolute deformation potential of semiconductors. *Appl. Phys. Lett.* **2006**, *88*, 042104.

https://doi.org/10.1021/acsomega.1c06367
ACS Omega 2022, 7, 11643−11653